Journal of Alloys and Compounds, 183 (1992) 59–74
JALCOM 7023

Structural peculiarities of the 123 and 2212 phases and materials based on them*

V. F. Shamrai, Yu. V. Efimov, A. A. Babareko, G. M. Leitus, S. A. Sibirtsev and A. I. Shulgin
A. A. Baikov Institute of Metallurgy of the USSR Academy of Sciences, Moscow (Russia)

(Received June 6, 1991)

Abstract

The refinement of structure parameters, chemical composition and T_c of mono- and polycrystalline $YBa_2Cu_3O_{7-x}$, $GdBa_2Cu_3O_{7-x}$, $DyBa_2Cu_3O_{7-x}$ and $Bi_2Sr_2CaCu_2O_{8+x}$ samples illustrate sharp correlations of the peculiarities of the crystal structures with the oxygen content and T_c level. Crystal anisotropy of the yttrium- and bismuth-based high-temperature superconducting 123 and 2112 phases under cold and warm plastic strip deformation gives rise to the formation of a basal texture, the perfection and stability of which are determined by the conditions of deformation, and subsequent annealing and phase transformations. The T_c level of polycrystalline materials depends slightly on the formation of basal texture and is determined by their substructure. The formation of shear texture in the yttrium-based high-temperature superconducting strips drastically decreases their T_c.

1. Introduction

The continued search for superconductors with high T_c, beginning virtually with the discovery of the phenomenon of superconductivity in 1911 by Onnes, was completed in 1986 when Bednorz and Mueller revealed that superconducting copper oxides are high-temperature superconductors (HTSCs) [1]. That the oxide superconductors can reach high T_c was suggested by Matthias (see ref. 2). In parallel with the investigations of superconducting A15 phases, carbides, nitrides, borides and other metal compounds, the superconductivity of oxides was intensively studied in recent years [3–5]. Along with these studies of superconducting oxides – $SrTiO_3$ [6], cubic spinels $LiTi_2O_4$ [7], complex oxides $BaPbO_3$ and $BaPiPbO_3$ [8, 9], niobium mono-oxide [10] and others [3] – the discovery of HTSCs was preceded by the investigation of superconducting ionic copper chlorides [11] and A15-phase-based composites, as well as other superconducting substances with dispersed copper inclusions [12, 13].

Unprecedented in its intensity, the study of superconductors on the basis of oxide ceramics has unfolded in two directions of structural investigations:

*Dedicated to Professor W. Bronger and Professor Ch. J. Raub on the occasions of their 60th birthdays.

0925-8388/92/$5.00

HTSC structure peculiarities that occur with different oxygen contents, which are extremely important for understanding the mechanisms of superconductivity; and the study of texture formation processes, which turned out to be decisive in the development of the high critical current materials. In the present paper, among the HTSCs with T_c higher than the boiling temperature of liquid nitrogen, these problems are examined in detail for $YBa_2Cu_3O_{7-x}$ (123) and $Bi_2Sr_2CaCu_2O_{8+x}$ (2212) phases.

The main crystal structure elements of the 123 phases are the CuO_2 planes consisting of Cu2, O2 and O3 sites (Fig. 1), and Cu1–O4 chains arranged on the basal plane. Since Z for Cu2 is somewhat less than Z_{O2} and Z_{O3} these planes are corrugated such that atoms O2 and O3 are almost coplanar. The Cu2 atoms are displaced from these planes towards O1 atoms by about 0.25 Å; nevertheless, the Cu2–O1 distance, as a rule, is distinctly larger than that from O1 to Cu1. Therefore, instead of Cu1–O4 chains, one frequently considers the CuO_4 quadrangular chains consisting of Cu1, O1 and O4 atoms. In most work it is assumed that the carriers that predominate in superconductivity are localized mainly on the CuO_2 planes. These systems could be described by the two-dimensional Hubbard model [14–17]. Their ground state is an insulator, and their compounds are metallic and superconducting when they are hole doped.

The crystal structure of the superconducting 123 phases may be regarded as that formed by packing along the c axis of the triple layers composed from the CuO_5 pyramid sheets turned with their apexes to the chains. It has been experimentally confirmed that the interaction between CuO_2 planes belonging to different elementary cells significantly affects the value of T_c [18].

The crystal structure of 2212 phases (Fig. 2) has as its main element two layers of the CuO_5 pyramids turned with their bases to each other. This structure is similar to that of 123 phases, but with the difference that such neighbouring layers are shifted by half of a period and that double Bi–O planes, rather than Cu–O chains, are arranged between the layers.

The variations in the superconducting characteristics of HTSC oxides due to their chemical composition, sintering conditions and other technological factors are determined by correlation of these properties, not only by the peculiarities of their crystal structure, but also by the pronounced crystallographic anisotropy of these compounds. The latter is manifested in the strong variation of the critical field and current characteristics depending on the crystal orientation, crystallographic texture and morphological texture of the polycrystalline samples.

In attempts to develop high critical current materials an understanding of the HTSC deformation and texture formation mechanisms when HTSCs are treated at high pressures is of great importance. The mono- and polycrystalline 123 and 2212 HTSCs belong to the class of materials with high susceptibilities to brittle fracture [19]. Owing to a pronounced anisotropy of the HTSC properties the powders [20, 21] acquire, upon crystal breaking, the non-axial shape of particles with a preferential orientation of plane

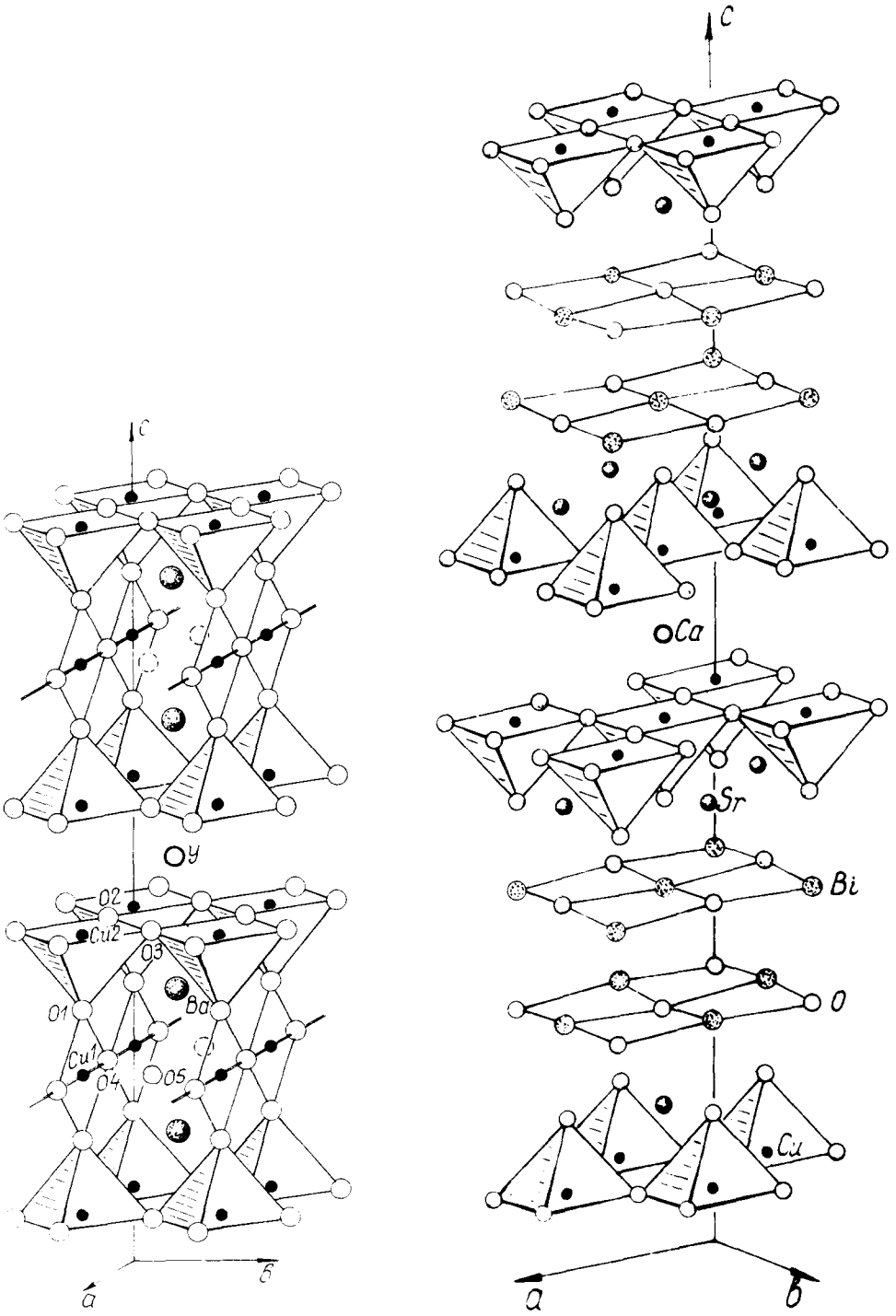

Fig. 1. Fragment of the $YBa_2Cu_3O_7$ structure.

Fig. 2. Fragment of the $Bi_2Sr_2CaCu_2O_8$ structure.

fracture. During deformation (single-axial compression, rolling) the yttrium- and bismuth-based HTSC materials acquire, as a rule, a basal (001) texture [22, 23]. Apart from its effect on texture formation the influence of pressure upon the lattice parameters of superconducting phases is also significant and the substructure diminishes the oxygen content and provides evidence of their chemical instability [22–26]. Owing to a strong critical current anisotropy in the HTSC crystals [27] the texture significantly affects the current characteristics of wires, strips and cables [21].

The present paper reports on correlations of the crystal structure peculiarities, oxygen content, texture and T_c of real mono- and polycrystalline samples and fine yttrium- and bismuth-based HTSC strips.

2. Materials and experimental details

The polycrystalline $YBa_2Cu_3O_{7-x}$ (123 phase with orthorhombic and tetragonal structure) and $Bi_2Sr_2CaCu_2O_{8+x}$ (2212 phase) samples were synthesized through a solid state reaction from mixtures of oxides, carbonates and nitrides at 750–1100 °C (0.5–100 h) in air and in flowing O_2 with an intermediate milling (from 2 to 6), with a cooling rate between 4 and 200 °C min^{-1}. The yttrium- and bismuth-based HTSC strip samples were prepared by rolling the fine powders of 123 orthorhombic phases ($T_c = 85$–93 K) and 2212 ($T_c = 80$–83 K) with carbon plastifier. The $YBa_2Cu_3O_{7-x}$, $GdBa_2Cu_3O_{7-x}$, $DyBa_2Cu_3O_{7-x}$ and $Bi_2Sr_2CaCu_2O_{8+x}$ crystals with sizes between 50 μm and 4–8 mm were grown by programmed polythermic and isothermic annealing. (In addition to our own samples, some of the crystals of these compounds used for the X-ray investigations were synthesized in the laboratory of Professor N. E. Alekseevskii.)

The metal and carbon contents were determined by chemical analysis, and the oxygen content by activation analysis. Electron microprobe determination of the metallic components in the monocrystals was carried out with a Camebax Microbeam microanalyser using the standard method; oxygen determination was carried out with the ultralong-wave Spectrozond microanalyser developed at the Baikov Institute of Metallurgy of the USSR Academy of Sciences and intended for precise spectral investigations in the wavelength range from 1.8 to 30 nm [28, 29].

The application of concave diffraction gratings as dispersive elements and windowless secondary-electron (channeltron) multipliers with open photocathodes used instead of flow proportional counters are the main differences between the Spectrozond microanalyser and the commercial device. A short-wavelength filtration system, based upon total external reflection, considerably increases spectrum contrast and eliminates the overlapping of the highest-order short-wavelength diffraction lines with analytical lines. In the spectrometers a new X-ray–optical Rowland focusing scheme is realized. A silicon dioxide crystal was used as a sample for comparison. The oxygen determination threshold in a HTSC using Spectrozond is 0.03–0.04 mass%, with an accuracy

of determination of 4 rel.%. The microstructure of alloys and strips was studied using a JSMU-3 scanning electron microscope. The T_c was determined using the inductive method and, in a few cases, the resistive method at temperatures of 77 K or more.

The X-ray investigation of polycrystalline samples has been carried out using an automatic DRON-3M diffractometer controlled by an IBM PC AT. Phase composition was analysed using the JCPDS database, literature data and the results of our investigations of the Y–Ba–Cu–O and Bi–Sr–Ca–Cu–O phase crystal structures. A set of intensities of the X-ray crystal reflections was collected with a Syntex PI diffractometer (Mo Kα radiation, $\theta/2\theta$ scanning). The structures were refined by an Aren complex [30] using the method of least squares in a full matrix approximation.

As is known, the study of the material texture of the 123 and 2212 phases involves certain experimental difficulties. The X-ray diffraction spectra of 123 and 2212 phases have no individual reflections applicable for a study of texture. All reflections are divided into overlapping groups with intervals of 0.3° for the 123 phase and 1–2.5° for the 2212 phase. The texture of yttrium- and bismuth-based HTSC strips was investigated by the method of direct pole figures (DPFs) from total reflections using an automatic DART UMI diffractometer with Cu K radiation. A method of DPFs for yttrium-based HTSC has been described earlier [29]. To determine the type of texture and preferred directions in the yttrium-based HTSC strips we used a group of (013)+(110)+(103) reflections. In order to estimate the perfection of the component of the basal texture, scattering angle and relative intensity at the maximum point, we used the group of reflections (014)+(005)+(104). For bismuth-based HTSC strips the DPFs were constructed from the total reflections (157)+(166)+(148) and (0 0 10)+(164) (indices in a cell with $b' = 6b$). In general, for determining the texture of the 2212 phase material the group of reflections presented in Table 1 is more suitable. This table also lists the positions of the texture maxima (angle α) on the different types of pole figures, estimated on the assumption of the presence of a basal texture in the material and determined by the angle φ between the basal and reflecting planes.

3. The results of structural investigations

The variations in the interatomic distances with increase in the oxygen deficiency in $GdBa_2Cu_3O_{7-x}$ are similar to those found earlier for $YBa_2Cu_3O_{7-x}$ [31] as determined by the refinement of the structural parameters (Table 2). The triple layers formed by CuO_5 pyramids, turned with their apexes towards the Cu1–O4 chains, are elongated. The CuO_5 pyramids are elongated such that their tops approach the chains, and the asymmetry in the position of apical O1 atoms is increased. The oxygen concentration decreases mainly because of the occupancy of the positions in the basal plane. Hence an

TABLE 1

The orthorhombic 2212 phase structure reflection group for determination of texture

hkl	I/I_0 (%)	2θ[a] (deg)	φ[b] (deg)	Maximum on pole figure
008	48.5	23.20	0	Main
151		23.20	82.9	–[c]
144	2.1	24.0	61.1	Absent
0 0 10	35.7	29.15	0	Main
164	7.7	28.45	65.7	Pronounced, complementary
091	7.5	29.72	84.4	–
0012			0	Main
168			47.9	Traces
204; 0104	5.8	35.15	70.5	–
159			41.7	Present
155	100	27.52	58.0	Main
164	7.7	28.45	65.7	Absent
16		26.5	77.2	–
119	4.0	26.5	7.2	Traces
157	74.5	31.0	48.8	Main
091	7.5	29.72	84.4	–
166			55.8	Introduce asymmetry into the main maximum

[a]Cu Kα radiation.
[b]Angle between the basic and reflecting planes.
[c]Dash corresponds to a lack of maximum within a pole figure.

increase in the Ba–Ba distance is correlated with the attenuation of screening of the Ba–Ba interaction. The occupancy of the Cu2 position for both large and small oxygen concentrations is close to unity. This result is in accordance with the knowledge of CuO_2 planes as elements that are slightly affected by different factors.

From our point of view the most significant variation in the $GdBa_2Cu_3O_{7-x}$ structure with decreasing x lies in the coming together of the main structure elements – CuO_4 chains and CuO_2 planes, which results in three-dimensional layer compression. Some increase in the Cu1–O1 distance (Table 2) does not compensate for this variation. Such a convergence should be considered to be the result of increasing the plane–chain interaction and the interaction between planes belonging to different cells which, as was mentioned above, is important for superconductivity in these systems. Attention should also be given to the fact that the O1, Cu1 and Cu2 atoms belong to different planes and are shifted towards one another and, as a result, there could be a change in the asymmetry of charge distribution along the c axis [32]. In the Hubbard model these effects can significantly modify the effective Coulomb potential and, hence, T_c.

The local density of states calculations point to the fact that in $YBa_2Cu_3O_7$ the hole density is different for chains and planes. They are linked via a

TABLE 2

Interatomic distances and Gd–Ba–Cu–O crystal structure parameters[a] before and after oxidation

	Distance (Å)	
	$GdBa_{1.96}Cu_{2.76}O_{6.4}$[b]	$GdBa_{1.97}Cu_{2.80}O_{6.9}$[c]
Cu1–O1	1.800(14)	1.835(10)
Cu1–O4	1.944(0)	1.945(0)
Cu2–O1	2.412(14)	2.312(10)
Cu2–O2	1.954(0)	1.959(1)
Cu1–Cu2	4.212(1)	4.146(1)
Cu2–Cu2	3.349(2)	3.374(2)
Ba–Ba	4.523(0)	4.340(0)
Ba–O1	2.787(2)	2.767(1)
a	3.887(1)	3.878(2)
b	–	3.890(1)
c	11.773(3)	11.667(6)

[a]Full structure parameters will be published elsewhere.
[b]$R = 3.9\%$; 371 independent reflections.
[c]$R = 4.2\%$; 694 independent reflections.

common Fermi level and the chains act merely as hole dopants for the CuO_2 planes [33]. Thus the superconductivity depends on the carrier concentration in the CuO_2 planes created by charge transfer from the chains playing the role of a charge reservoir. As the oxygen deficiency increases, the carrier concentration in the planes is changed and the observed variations in interatomic distances fix this charge transfer [34–36]. The bond lengths turn out to be rather sensitive to this process. From the estimates of the charge on chemical bonds associated with copper carried out for different oxygen concentrations in $YBa_2Cu_3O_{7-x}$ with the use of interatomic distances refined by the neutron diffraction method [35] it follows that the decrease in positive charge associated with copper in the plane is 0.03 electron per copper ion and 0.05 electron per copper ion near the sharp variations of T_c at $x = 0.3$ and $x = 0.5$ respectively. According to ref. 36, charge transfer in $YBaCu_3O_{7-x}$ is fixed by such distances as Cu1–O4, Cu2–O1, and Cu2–Cu2 best of all. From the results of refinement (the structure parameters listed in Table 2) it is seen that the character of the distance variation with increasing x in $GdBa_2Cu_3O_{7-x}$ is similar to that described above and this makes it possible to assume that a reservoir-plane concept is applicable for this compound too.

The $DyBa_2Cu_3O_{6.8}$ crystal undergoes a superconducting transition in the interval from 50 to 18 K. At the same time the structure of this compound is satisfactorily refined in the tetragonal system (space group, *P4/mmm*; *R* factor, 0.032). Three-dimensional scanning in the region of reciprocal space around (220) (*h*00) and (00*l*) has revealed an abnormal intensity distribution in proximity to these reflections. The form of the reflections can be explained by the assumption that the crystal under investigation consists of orthorhombic

twin domains separated by sufficiently wide interlayers, where the periods a and b vary smoothly. In other words the average occupancy of oxygen positions ($\frac{1}{2}$ 0 0) and (0 $\frac{1}{2}$ 0) is gradually changed from zero to unity and sequentially a and b change from 3.83 to 3.89 Å (estimated from the extension of reciprocal lattice points), yielding the pattern of a pseudotetragonal crystal with $a=b=3.868$ Å.

The T_c dependence on oxygen content in $YBa_2Cu_3O_{7-x}$, as is known, is non-monotonic. This dependence has two plateaux near 90 and 60 K which are fixed respectively for $0<x<0.2$ and $0.4<x<0.55$. Further increase of x gives rise to a sharp decrease of T_c, and for $x\geqslant 0.65$ the superconductivity disappears. With the use of electron microscopic methods it was established that, as oxygen is removed from the chains, two- and three-dimensional superlattices are formed due to ordering of the "filled" and "empty" (with respect to oxygen) chains [37]. At the oxygen concentration corresponding to the plateau with $T_c=60$ K a three-dimensional long-range oxygen-ordered structure ($2a_0\times b_0\times 2c_0$) is obtained. The appearance of this phase is caused by a full lack of oxygen in each second chain in the a and c directions. This phase is found over a relatively wide interval of concentrations ($0.2<x<0.7$) and, as a rule, coexists with less stable phases where the oxygen-filled or "vacant" Cu1–O4 chains in the basal planes alternate in the a direction with periods $3a_0$, $4a_0$ and $5a_0$. In the general case, order of the chain alternation along the c axis is absent and superstructure is not realized in the volume. In the 123 phases other types of superstructure [38–41], *e.g.* the superstructure $2^{1/2}a_0\times 2^{3/2}b_0\times c_0$, develop due to a structure parameter modulation [40] as revealed by the electron microdiffraction method. Our experiments on the X-ray diffraction of $YBa_2Cu_3O_{6.6}$, $GdBa_2Cu_3O_{6.3}$ and $GdBa_2Cu_3O_{6.9}$ crystals have not revealed any superstructure reflections.

In Bi–Cu–O 2212 crystals the X-ray reflections occurring due to structure parameter modulation are clearly observed. The $Bi_{1.99}Sr_{1.60}Ca_{1.00}Cu_{1.83}O_{6.83}$ crystal structure refined by a full-matrix least-squares method to $R=0.065$ with the elementary cell periods $a=5.405$ Å, $b_0=5.402$ Å and $c=30.766$ Å (space group *Cccm*, 114 independent reflections) has led to a model analogous to that in ref. 42. The scattering factors at bismuth positions turned out to be lower, and at the strontium positions were higher, as compared with the data following from the results of microprobe analysis (Fig. 2). The superstructure reflections correspond to a commensurate modulation along the b axis with the period $b=5b_0$. As the set of structure amplitudes is small and the crystal shape ($170\times 140\times 2$ μm^3) is drastically anisotropic, the crystal structure refinement in the model with the elementary cell with $b=5b_0$ was rather complicated. At the same time an analysis of intensities enables us to reach conclusions concerning the character of the structure parameter variations within a "large" cell.

A set of Bi–Cu–O experimental intensities not including 232 subcell reflections had 142 superstructure reflections with $k=5n\pm 1$ whose intensity is considerably weaker. No reflection with $I(hkl)>3\sigma$ and $k=5n\pm 2$ has been revealed. A structure factor $F(hkl)$ can be presented as a sum of contributions

of the structure factors of atoms belonging to five neighbouring subcells with $b = b_0$:

$$F(hkl) = \sum_{m=1}^{5} \sum_{j}^{N_a} f_j \exp[2\pi i(hx_{jm} + ky_{jm} + lZ_{jm})] \tag{1}$$

where m and N_a are the number of the subcell and the number of atoms in it respectively; f_i, x_{jm}, y_{jm} and z_{jm} are the atomic and position parameters.

Assuming that $y_j^m = y_{im} - (m-1)/5$, then

$$F(hkl) = \sum_{m=1}^{5} \exp[2\pi ik(m-1)/5] \tag{2}$$

where F_m is the contribution to the structure factor from the subcell m:

$$F_m = \sum_{j}^{N_a} f_j \exp[2\pi i(hx_{jm} + ky_j^m + lZ_{jm})] \tag{3}$$

A satisfactory refinement of the structural parameters in the model with $b = b_0$ makes it possible to assume that the difference in the atomic parameters of the five neighbouring subcells is not large, and then

$$\begin{aligned} &|F_i| - |F_j| \ll |F_i| \qquad i \neq j \\ &|F_i + F_j| \approx |F_i| + |F_j| \end{aligned} \tag{4}$$

Then, for $k = 5n$, $|F(hkl)| \approx \Sigma_{m=1}^{5} |F_m|$, and for $k \neq 5n$ the values of $F(hkl)$ can be presented as a sum of vectors (Fig. 3).

Taking into account (as follows from experiment) that, for $k = 5n \pm 2$, $F(hkl) = 0$, and, for $k = 5n \pm 1$, $F(hkl) \neq 0$, then

$$(|F_2| - |F_5|) \sin \frac{4\pi}{5} + (|F_3| - |F_4|) \sin \frac{2\pi}{5} = 0 \tag{5}$$

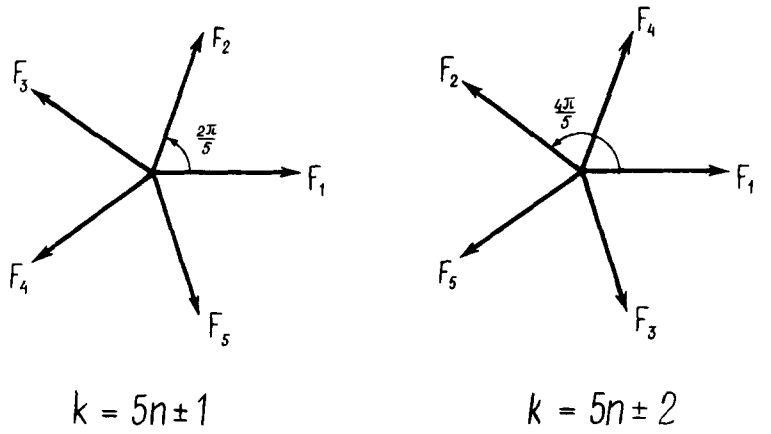

Fig. 3. Vector diagrams of the contribution of structure factors F_{hkl} for $k = 5n \pm 1$ and $k = 5n \pm 2$.

$$|F_1| + (|F_2| + |F_5|) \cos \frac{4\pi}{5} + (|F_3| F_4|) \cos \frac{2\pi}{5} = 0 \quad (6)$$

Equations (4) and (5) yield that $|F_2| \approx |F_5|$ and $|F_3| \approx |F_4|$. Then, assuming that $|F_1| = F$, and $|F_2| = |F_5| = \alpha F$, where α is close to unity, from eqn. (6) it follows that $|F_3| = |F_4| = (2.6\alpha - 1.6)F$. Thus, the conditions limiting possible reflection of the type $k = 5n \pm 2$ can be the result of periodic variations in the contributions to the structure factor from different subcells F_m with relatively small amplitude.

An appearance of modulated structure in the bismuth 2212 phase is caused by vacancies in the bismuth and strontium layers, by partial substitution of Bi atoms for strontium and bismuth for calcium as well as calcium and strontium for calcium, and by atomic displacements in the bismuth, strontium and calcium layers [42, 43]. An analysis of the results of refining the structural parameters of one average cell makes it possible to consider that we have a periodically varied (with relatively small amplitude) occupancy of bismuth and strontium positions along the b direction with the period $5b_0$.

4. Texture and anisotropy of the yttrium- and bismuth-based HTSC strip properties

The two-dimensional character of the main fragment of structure to which the authors attribute the presence of superconductivity in the 123 and 2212 phases determines a sharp anisotropy of the critical current of these superconductors. As is known, the ratio of the critical current values along and perpendicular to the c axis reaches about 10^3 [27]. So while developing the materials with high current capability a great deal of attention is paid to forming favourable texture in which the basal plane is oriented in the direction of current flow. We have considered these questions in detail in connection with rolling the yttrium- and bismuth-based plastified powders.

We have previously reported in refs. 23 and 44 that the rolling of the plastified yttrium-based HTSC powders can lead to production of rather high-strength flexible strips with good (00l) [hk0] basal texture. The texture becomes stronger as the extent of deformation is increased. The texture has an axial component (with the rotation axis around a normal to the rolling plane); the orientations (011) [010], (001) [110] and (001) [210] can also be identified.

The rolling of 2212-phase powders also leads to the formation of basal texture (Fig. 4). With 90–96% deformation the pole density is $P_{(0\,0\,10)} = 15$ arbitrary units (scattering angle, about 15°). While studying the texturegrams of bismuth-based HTSC superstructure reflections are clearly observed. By means of these reflections it is possible to obtain additional information on the texture. Thus (Fig. 5) the use of the reflection group (0 0 10)+(164), which includes a superstructure (164) reflection, makes it possible with one pole figure to analyse both the basal texture intensity, according to the

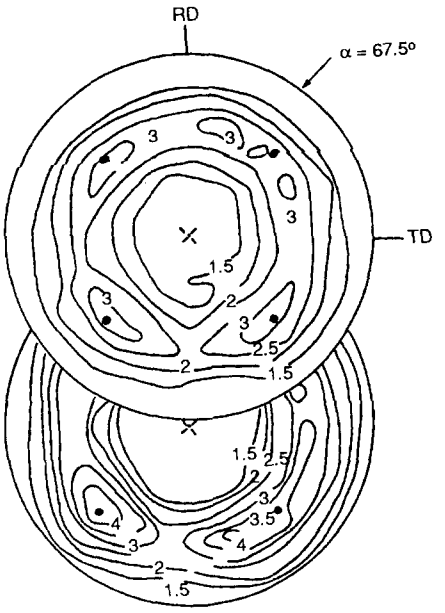

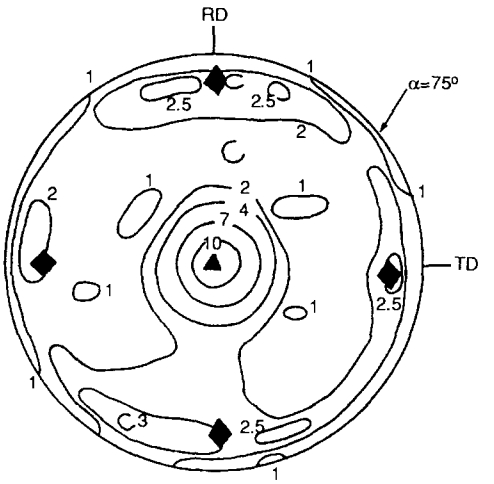

Fig. 4. (117) pole figure of the bismuth-based HTSC samples deformed by 94% and annealed at 840 °C for 100 h. ●, (001) [100] (001) [010].

Fig. 5. (0 0 10)+(164) pole figure of the bismuth-based HTSC strip after rolling with a deformation of 94% and annealing for 24+100 h at 450 °C, showing the texture maxima of the (001) [110] orientation produced from the main (0 0 10) reflection (▲) and superstructure (164) reflections (■).

central maximum from the (0 0 10) reflection and, according to the position of the maxima on the periphery from the (164) reflection, to reveal the texture axis arranged in the rolling direction.

In the pole figures of the yttrium-based HTSC strips produced by rolling with extensive deformation the orientation (139) [18 3 1], whose indices in the b.c.c. subcell are (133) [611] are exhibited (Figs. 6(a) and 6(b). This orientation deviates by 13° from the Goss orientation (011) [100] describing the shear deformation texture over the close-packed (011) planes in metals with the b.c.c. structure. Such a texture in yttrium-based HTSC strips is exhibited by increasing the pole density in the centre of the DPF (013)+(110)+(103). The metal atoms of the 2212 phase form an f.c.c. subcell. By analogy with the shear texture observed in the yttrium-based HTSC strips a shear texture formation was expected over the close-packed (111) planes of the f.c.c. subcell, *i.e.* the (115) planes of the 2212-phase cell. At the applied deformation the pole figures of the bismuth-based HTSC strips were free of shear texture contributions.

Strip annealing can essentially modify the texture. The yttrium-based HTSC strips annealed at the temperatures close to the structural transformation exhibit these effects more clearly. Strip annealing at temperatures up to 400 °C does not make essential modifications to their texture. A short annealing

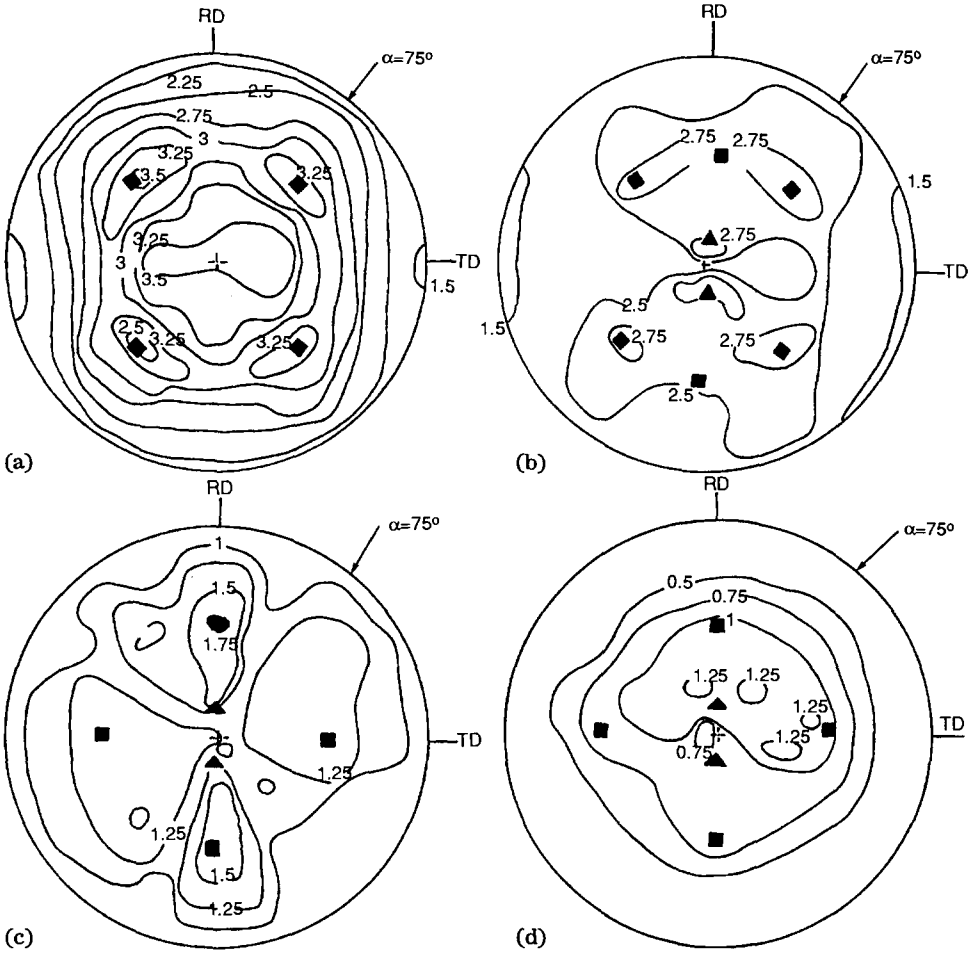

Fig. 6. DPFs of the cold-deformed yttrium-based HTSC strips from the total (013) + (110) + (103) reflection at (a) $2\theta = 32.8°$ and (b) $2\theta = 32.3°$ as well as after annealing at (c) 450 °C for 110 h and (d) 600 °C for 24 h.

at 400–500 °C does not change the type of texture, somewhat weakens it and stimulates transition from (001) [110] to (001) [100] and (001) [010] orientations. This temperature range corresponds to a maximum diffusive mobility of oxygen atoms and intense oxygen saturation of the 123 phase [45, 46]. An increase in the duration of low-temperature annealing (450 °C) leads to the appearance of a set of orientations which are intermediate between the basal and (139) orientations. The type of texture in samples annealed at 400–500 °C is of a "tab" character on the yttrium-based HTSC strips (Fig. 6(c)). This texture can be explained on the basis of the theory of compromise grain growth. This theory attributes the character of the texture variation with more active growth of those recrystallized nuclei which can grow by absorbing all or some components of the initial multicomponent texture [47]. These are those recrystallization nuclei whose orientations hit

a spread of orientations between two (or more) components of the initial texture.

An abnormally strong decrease in basal texture is observed during annealing of the rolled yttrium-based HTSC strips at 600–650 °C (Fig. 6(d)). This decrease appears to arise from the lattice instability near the phase transformation from orthorhombic to tetragonal modification [48] of the 123 compound. Annealing at higher temperatures (900–950 °C) leads to weak texture scattering. By keeping a well-formed basal texture such an annealing leads to an increase in the orthorhombic distortion due to oxygen saturation which is, however, smaller than for the low-temperature annealing.

The texture of the bismuth-based HTSC strip is more stable on annealing. Annealing at $T < 600$ °C virtually does not affect this texture. Annealing in the temperature range 600–840 °C for 24–100 h even increases its perfection (Table 3); longer periods at these temperatures cause its weakening but even after 100 h it remains distinct enough. Annealing at $T > 840$ °C is accompanied by an abrupt decrease in texture; the smooth superconducting transition observed in this case makes it possible to consider that these temperatures lead to structure evolutions typical for the temperatures near the melting point (850 °C, incongruently [49]).

As is known, the value of T_c and the superconducting transition width of HTSCs greatly depend on such factors as substructure, concentration of the different types of defect, oxygen content, orthorhombic distortion and so on. All these parameters can be significantly varied in the course of strip rolling and annealing. At the same time our experiments indicate that there is a certain regularity of T_c variation *vs.* the type of texture. Rolling of plastified powders of the 123 and 2212 phases, even at relatively small extents of deformation, leads to formation of a well-formed basal (00*l*) [*hk*0]

TABLE 3

Variations in the lattice parameters[a] and T_c in superconducting strips of the 2212 phase

Conditions of material production	Degree of texturing[b]	a (Å)	c (Å)	T_c (K)
Initial powder		5.40	30.6	86
Deformed strip				
85–90% deformation	4	5.383	30.52	85.4
96% deformation	4.5	5.381	30.48	85
Annealing in air				
600 °C, 24 h	5	5.376	30.48	85
720 °C, 24 h	10	5.371	30.59	88.1
840 °C, 100 h	8	5.374	30.56	89.9
850 °C, 9 h	3	5.378	30.49	77–95[c]

[a]As the a and b periods of the orthorhombic 2212-phase lattice are close, the calculation is carried out according to a pseudotetragonal structure.
[b]Expressed by the relation $I_{(008)+(151)}/I_{(155)}$.
[c]Smooth transition with very large hysteresis.

texture or packing texture. Values of T_c determined as $T_c = T_c\ (\rho_{N/2})$, where ρ_N is the normal state electroresistance near the superconducting transition, is not essentially decreased in this case. As soon as the shear component (139) [1$\bar{8}$ 3 1] appears on pole figures, T_c is noticeably decreased. Such a dependence becomes clear if account is taken of the fact that during the packing texture formation a crystal cleavage along (00l) planes, and particle redistribution with the basal plane orientation along the direction of rolling, occurs. The main structural element which plays an essential role in superconductivity of these compounds, the CuO_2 planes, is not disturbed. Growth of the superconducting transition width is perhaps the result of the internal stress formation as it usually takes place in the A15 superconductors and Chevrel phases. The formation of the (139) [$\bar{8}$ 3 1] component is related to the development of defects deforming the CuO_2 planes and, hence, to the decrease in T_c.

5. Conclusions

Our investigations carried out on the structure of a set of superconducting 123 and 2212 copper oxides, and studied more intensively because of their practical application, correspond to the known predominant role of the CuO_2 planes in superconductivity. A space between the CuO_2 planes can be considered as a reservoir from which the planes are doped with hole carriers. The change of copper oxidation state can regulate this process. The interatomic distances such as Cu1–O1, Cu2–O1 and Cu2–Cu2 appear to be rather sensitive indicators fixing the charge transfer between Cu–O chains and CuO_2 planes. The characteristic feature of 2212 superconductivity is structural modulation, the formation of which is a consequence, perhaps, of the difference between the CuO_2 planes and Bi–O layer periods. A disturbance of the perfection of the main structural element to which the presence of superconductivity may be attributed, *i.e.* the CuO_2 planes, as a result of external effects (for example, shear over (139) planes during rolling of the $YBa_2Cu_3O_{7-x}$ samples) results in the suppression of superconductivity.

References

1 J. G. Bednorz and K. A. Mueller, *Z. Phys.*, *64* (1986) 189.
2 Ch. J. Raub, *J. Less-Common Met.*, *137* (1988) 287.
3 E. Beck, A. Ehrmann, B. Krutsch, S. Kemmler-Sack, H. R. Khan and Ch. J. Raub, *J. Less-Common Met.*, *147* (1989) L17.
4 *J. Less-Common Met.*, *62* (1978), Special Issue dedicated to B. T. Matthias.
5 A. R. Sweedler, J. K. Hulm, B. T. Matthias and T. H. Geballe, *Phys. Lett.*, *19* (1965) 82.
6 Ch. J. Raub, A. R. Sweedler, M. A. Jensen, S. Broadston and B. T. Matthias, *Phys. Rev. Lett.*, *13* (1964) 746.
7 M. J. Dayle, J. K. Hulm, C. K. Jones, R. C. Miller and A. Taylor, *Phys. Lett. A*, *26* (1968) 604.
8 V. V. Bogatko and Yu. N. Venevchev, *Fiz. Tverd. Tela*, *22* (1980) 1211 (in Russian).

9 A. W. Sleight, J. Z. Gillson and P. E Bierstedt, *Solid State Commun., 17* (1975) 27.
10 P. E. Jones, J. R. Shanks and D. K. Finemore, *Phys. Rev. B, 6* (1972) 835.
11 N. B. Brand, S. V. Kuvshinnikov, A. P. Rusakov and M. V. Semenov, *JETP Lett., 27* (1978) 37 (in Russian).
12 H. Winter, *Br. Patent 2,557,840,* June 30, 1977.
13 Ch. J. Raub and E. Raub, *Z. Phys., 186* (1965) 310.
14 P. W. Anderson, *Science, 235* (1987) 1196.
15 B. K. Chakraverty, M. Avignon and D. Feinberg, *J. Less-Common Met., 150* (1989) 11.
16 F. E. Hirsh, *Physica C, 158* (1989) 326.
17 D. Schmeltzer, *J. Phys. G, 1* (1989) 2821.
18 Q Li, X. Xuxi, X. D. Wu, A. Jaam, S. Valamannati, W. L. McLean, T. Venkatesan, R. Ramesh, D. M. Hwang, J. A. Martinez and L. Nazar, *Phys. Rev. Lett., 64* (1990) 8086.
19 Q. Ni, A. Li, Y. Li and Q. Kong, *Chinese J. Phys. Lett., 6* (1989) 321.
20 V. F. Shamrai, *Fizikokhimiya y Tekhnologiya Vysokotemperaturnykh Sverkhprovodyaschchikh Materialov, (Physical Chemistry and Technology of High-T_c Superconducting Materials),* Nauka, Moscow, 1989, p. 19 (in Russian).
21 K. Watanabe, K. Noto and H. Morita, *Cryogenics, 29* (1989) 263.
22 A. Luzhnikov, L. L. Miller and K. M. McCallum, *J. Appl. Phys., 65* (1989) 3136.
23 V. F. Shamrai, Yu. V. Efimov, A. A. Babereko, F. R. Karelin, V. F. Choporov, T. M. Frolova and E. A. Myasinkova, *Sverkhprovodimost: Fiz. Khim., Tekh. (Superconductivity: Phys., Chem., Tech), 2* (1989) 18 (in Russian).
24 B. C. Hendrix, T. Abe, J. C. Borofko and J. K. Tien, *Appl. Phys. Lett., 55* (1989) 313.
25 G. S. Burkhanov, M. I. Bychkova, A. A. Korostelin and S. A. Lachenkov, *Fizikokhimiya i Tekhnologiya Vysokotemperaturnykh Sverkhprovodyashchikh Materialov (Physical Chemistry and Technology of High T_c Superconducting Materials),* Nauka, Moscow, 1989, p. 287 (in Russian).
26 N. S. Kispyi, T. A. Prikna and P. A. Nagornyi, *Fizikokhimiya i Tekhnologiya Vsokotemperaturnikh Sverkhprovodyashchikh Materialov (Physical Chemistry and Technology of High-T_c Superconducting Materials),* Nauka, Moscow, 1989, p. 289 (in Russian).
27 Yu. C. Bulyshev, G. A. Kuznetsov, Yu. V. Parfenov, S. V. Serykh and A. G. Shneider, *Sverkhprovdimost: Fiz., Khim., Tekh. (Superconductivity: Phys. Chem., Tech.), 3* (1990) 2529 (in Russian).
28 A. I. Shulgin, A. I. Kozlenkov, T. A. Bolokhova and V. G. Bogdanov, *Tezisy Dokl. Ch. M. Vsesoyuznogo Soveshchaniya po Rentgenovskoy Elektronnoy Skeptroskopii (Proc. XV All-Union Conf. on X-ray and Electron Spectroscopy),* LNPO Burevestnik, Leningrad, 1988, p. 112 (in Russian).
29 V. F. Shamrai, Yu. V. Efimov, A. A. Babareko, E. A. Myasinkova, T. A. Bolokhova and A. I. Shulgin, *Zavod Lab., 56* (1990) 60 (in Russian).
30 V. I. Andrianov, *Kristallografiya, 32* (1987) 228 (in Russian).
31 V. F. Shamrai, G. M. Leitus, O. G. Karpinsky, I. A. Kaskov, Yu. V. Efimov and S. G. Zhukov, *Proc. 12th Int. Plansee Seminar,* Vol. 1, Tyrolia, Innsbruck, 1989, pp. 717–723.
32 C. J. Fong, M. S. Wartak and S. N. Shelton, *Solid State Commun., 69* (1989) 219.
33 M. Avignon and K. H. Benneman, *Solid State Commun., 69* (1989) 999.
34 J. Tokura, J. B. Torrance, T. C. Huang and A. I. Nozzal, Phys. Rev, B, 38 (1988) 7156.
35 R. J. Cava, A. W. Hewat, B. Batlogg, M. Merizio, K. M. Rabe, T. J. Krajewski, W. F. Peck, Jr. and L. W. Rupp., Jr., *Physica C, 165* (1990) 419.
36 J. D. Jorgensen, R. W. Veal, A. P. Paulikas, L. J. Nowicki, G. W. Grabtree, H. Claus and W. P. Kowk, *Phys. Rev. B, 41* (1990) 1863.
37 S. Amelinckx, G. Van Tandeloo and J. Van Landuyt, *Solid State Ionics, 39* (1990) 37.
38 T. S. Shi J. Reyes-Gasga, C. Fanidis, S. Amelinckx, J. Van Landuyt and G. Van Tandeloo, *Micron Microsc. Acta, 20* (1989) 149.
39 T. Krekels, T. S. Shi, J. Reyes-Gasga, G. Van Tandeloo, J. Van Landuyt and S. Amelinckx, *Physica C, 167* (1990) 677.
40 T. Kemin, H. Meisheng and W. Yening, *J. Phys. G, 1* (1989) 1049.

41 M. Hervieu, B. Domenges, B. Raveau, M. Lost, W. R. McKinnok and J. M. Tarascon, *Mater. Lett., 8* (1989) 73.
42 K. Imai, I. Nakao, T. Kawashima, S. Sueno and A. Ono, *Jpn. J. Appl. Phys., 27* (1988) 1661.
43 V. Petricek, J. Gao, P. Lee and P. Coppens, *Phys. Rev. B, 42* (1990) 387.
44 V. F. Shamrai, Yu. V. Efimov, O. G. Karpinsky, G. M. Leitus, T. M. Frolova, E. A. Myasnikova, A. M. Postnikov, M. E. Saveljeva and Yu. L. Lipikhin, *J. Less-Common Met., 162* (1990) 181.
45 N. M. Kotov, O. A. Shlyakhtyn, N. V. Shipkov and Yu. V. Bogun, *Tezisy Sh Vsesoyuznogo Soveschehaniya po Probleme Diagnostiki Materialov VTSP (Proc. I All-Union Conf. on the Problem of Diagnostics in HTSC Materials);* Akademii Nauk S.S.S.R., Chernogolovka, 1989, p. 46 (in Russian).
46 Yu. F. Bychkov, A. M. Kharchenko, V. V. Mikhailov, I. I. Laptev, V. V. Ovcharov and E. I. Yakovlev, *Fizikokhimiya i Tekhnologiya Vysokotemperaturnykh Sverkhprovdyashchikh Materialov (Physical Chemistry and Technology of High-T_c Superconducting Materials)*, Nauka, Moscow, 1989, p. 179 (in Russian).
47 A. A. Babareko, *Itogi Nauki i Tekhniki, Seriya: Metallovedenie i Termicheskaya Obrabotka (Results of Science and Technology, Series: Metals Science and Heat Treatment)*, BINITI, Moscow, 1969, p. 5 (in Russian).
48 J. Sestak, *Thermochim. Acta, 148* (1989) 235.
49 P. Majewski, B. Freilinger, B. Hettich, T. Popp and K. Schulze, in H. Freyhardt (ed.), *High-Temperature Superconductors: Materials Aspects,* Deutsche Gesellschaft für Metallwerke, Garmisch-Partenkirchen, 1990, p. 111.